Institut für Angewandte Physik
der Universität Bonn
Wegelerstraße 8
53115 Bonn

Optical Phase Lock Loops and Raman-Cooling

Masterarbeit in Physik

von

Kohei Katayama

angefertigt im

Institut für Angewandte Physik,

vorgelegt der Mathematisch-Naturwissenschaftlichen Fakultät der Universität Bonn

(30, Dezember, 2010)

1. Gutachter: Prof. Dr. D. Meschede
2. Gutachter: Dr.P. D. Eversheim

Table of Contents

Chapter 1: Introduction

If the size of computer is reduced to the size of atoms, quantum mechanical effects may change the nature of computation. Such computer is called quantum computer and are expected to be a powerful tool for some important computational problems, like the prime factoring of large integers [1].

At the heart of quantum computation is the entanglement of many two-state systems called quantum bits (qubits), which form the register of the quantum computer. Creating and maintaining such an entangled state requires that the qubits are strongly coupled to one another and to an external field to produce the conditional-logic operations [2], yet coupling to other external influences must be minimized because it leads to decoherence. Quantum error correction and fault-tolerant computation promise to defeat the deleterious effects of decoherence, but only if the coupling to the environment is sufficiently weak. It is also required that coherence time is much longer than the time required for logic gate operation.

Several physical realizations of quantum computation have been proposed. One of the most promising is base on storing each qubit in the state of an ultra-cold trapped ion [3]. Ions interact strongly via their mutual Coulomb repulsion, thus allowing unitary manipulation of the qubits' joint state to be achieved with lasers. Because of their charge, however, the ions interact strongly with the environment, giving rise to decoherence channels from technical noise sources. Elements of quantum computation have also been implemented in standard NMR apparatuses [4] and in cavity QED [5], but these schemes are at present difficult to scale to many qubits. Solid-state systems, including quantum dots, have also been proposed for realizing quantum computation [6], but the strong interactions that exist in a condensed-matter environment make decoherence a difficult problem. Another system for implementing quantum logic gates is by using cold controlled collisions of trapped neutral atoms [2]. Such a system has two advantages: decoherence is suppressed because neutral atoms couple weakly to the environment, and operations can be performed in parallel on a large ensemble of trapped atoms, thus offering possibility for scaling to many qubits.

In our group, study is being conducted on entanglement of trapped neutral atoms. In this chapter, the current condition of experiment is briefly reviewed.

1.1 Cesium atom

Cesium (Cs) atom is chosen as our information carrier. Cs atom has stable hyperfine ground states which can be used to encode our qubit states and interacts with its environment weakly owning to its electric neutrality resulting in a long coherence time. Two hyperfine states $|0\rangle = |F = 4, m_F = 4\rangle$ and $|1\rangle = |F = 3, m_F = 3\rangle$ are chosen as the qubit states. A weak magnetic field of 3 G is applied in order to define the quantization axis. Initially Cs atoms are equally distributed among its magnetic sublevels of the F=3 state. Using pump lasers which have σ^+-polarization and connect F=3 and F=4 states to F'=4 state from which Cs atoms quickly decay, Cs atoms are stored in $|0\rangle$ state as shown in figure 1.1.

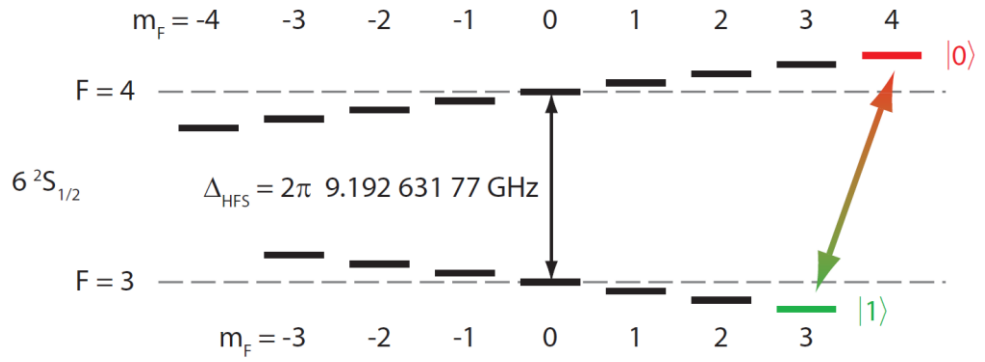

Figure 1.1: Zeeman splitting of the magnetic sublevels of the $6^2S_{1/2}$ ground state manifold of Cs. Our qubit states are stored in the outermost sublevels. Coherent transitions between the two states are driven by microwave radiation at a frequency of around 9.2 GHz.

1.2 Optical lattice and coherent manipulation of neutral atoms

In an optical lattice, neutral atoms can be trapped in the intensity maxima (or minima) of a standing wave light field due to the optical dipole force. An optical lattice is produced by two counter-propagating laser beams with linear polarization vectors enclosing an angle θ. Such a standing wave light field can be decomposed into a superposition of a σ^+ and σ^- polarized standing wave laser field, giving rise to lattice potentials $V_+(x,\theta) = V_{max}\cos^2(kx + \theta/2)$ and $V_-(x,\theta) = V_{max}\cos^2(kx - \theta/2)$. By changing the polarization angle θ one can thereby control the separation between the two potentials. When increasing θ, both potentials shift in opposite directions and overlap again when $\theta = n \cdot 180°$, with n being an integer. For a state-dependent transfer, two internal states of the neutral atom should be used, where one state dominantly experiences the $V_+(x,\theta)$ potential and the other state mainly experiences the $V_-(x,\theta)$ potential. Such a situation can be realized by tuning the wavelength of the optical lattice laser to a value between the fine structure splitting of the caesium D1 and D2 transitions. In our case, an atom in the state $|1\rangle = |F = 4, m_F = 4\rangle$ experiences only $V_-(x,\theta)$, whereas an atom in the state $|0\rangle = |F = 3, m_F = 3\rangle$ experiences both of the potentials. The latter condition is solved by tuning the wavelength of the optical lattice to a certain wavelength, called the magic wavelength, where $|0\rangle$ experiences almost exclusively the $V_+(x,\theta)$. Under such condition, by moving the centre of the potentials, we can shift the position of Cs atoms depending on its state. The polarization angle θ is controlled using a λ/4-waveplate and an Electro-Optical Modulator (EOM). The atoms are loaded onto the optical lattice at the temperature of around 10 μK after cooling by a standard magneto optical trap (MOT). The oscillation frequency of the optical lattice is $2\pi \times 115$ kHz.

1.3 Side-band cooling in axial direction

The trapped Cs atoms are cooled to the ground state of vibrational state by sideband cooling technique [7]. In sideband cooling a laser beam of frequency ω_L is incident on a two-level atom along the direction of the atomic motion with oscillation frequency ω_v. The absorption spectrum is composed of a carrier frequency ω_0 and sidebands spaced by ω_v. Cooling occurs when the laser is tuned to a lower sideband and when the oscillation frequency is much larger than radiative linewidth of the transition γ , $\omega_v \gg \gamma$. Under such condition, spontaneous

emission results in reduction of the atom's kinetic energy by $\hbar\omega_v$. With this technique, the Cs atoms are cooled to the ground state with a population of 97%.

1.4 Donut beam

The Cs atoms will be further trapped in radial direction by the use of a laser beam with a centre dark region, called a donut beam. The donut beam is produced by shining a laser bean onto a spiral phase plate which is a phase plate with an increasing thickness proportional to the azimuthal angle as depicted in figure 1.2.(a). The spiral phase plate causes destructive interference of the laser beam at the centre of the plate resulting in a dark region as in figure 1.2.(b). When the frequency of the laser beam is blue-detuned, the Cs atoms experience dipole potential proportional to the intensity of the donut beam and are trapped at the centre of the donut beam. The radial oscillation frequency Ω_{rad} of the trapped Cs atoms is related to the power P of the donut beam as $\Omega_{rad} \propto \sqrt{P}$. Currently the donut beam is not applied due to a lack of power after a tapered amplifier. When the tapered amplifier is properly applied, the intensity of 1 W and the radial oscillation frequency of $2\pi \times 20$ kHz are expected [8].

(a) (b)

Figure 1.2: (a) The structure of a spiral phase plate. The thickness of the plate increases proportional to the azumuthal angle. (b) Beam pattern of a donut beam.

1.5 Entanglement of neutral atoms and quantum gates

In quantum computation with trapped neutral atoms, entanglement is implemented by controlled cold collision. The cold collision is induced by the state-dependent control of neutral atoms by optical lattice as mentioned above. Suppose two atoms at lattice positions j and j+1, each of them with two internal levels $|1\rangle_{j,j+1}$ and $|0\rangle_{j,j+1}$. The result of the cold collision is given by

$$|1\rangle_j|1\rangle_{j+1} \rightarrow |1\rangle_j|1\rangle_{j+1},$$
$$|1\rangle_j|0\rangle_{j+1} \rightarrow e^{-i\phi}|1\rangle_j|0\rangle_{j+1},$$
$$|0\rangle_j|1\rangle_{j+1} \rightarrow |0\rangle_j|1\rangle_{j+1},$$
$$|0\rangle_j|0\rangle_{j+1} \rightarrow |0\rangle_j|0\rangle_{j+1},$$
$$\phi = \frac{1}{\hbar}\int_{-\tau}^{\tau} dt\Delta E(t),$$
$$\Delta E(t) = \frac{4\pi a_s \hbar^2}{m}\int dx \left|\psi_{|1\rangle,j}(x,t)\right|^2 \left|\psi_{|0\rangle,j+1}(x,t)\right|^2,$$

where ϕ is the interaction phase due to coherent interaction between the two atoms, a_s is the s-wave scattering length between the state $|1\rangle$ and $|0\rangle$, m is the mass of Cs atom, and $\psi_{|\beta\rangle,i}(x,t)$ is the normalized wave function of an atom at a lattice point I in qubit state β. The kinetic

phase due to kinetic energy of an atom is incorporated in the definition of the states. These logics are the basis of quantum gates. One of the simplest examples of quantum gate is Controlled-NOT (CNOT). Operation of CNOT is shown in figure 1.3. In CNOT, the following sequence of operations is applied: (1) a $\pi/2$-pulse brings all atoms into a superposition of the qubit states; (2) the lattice is shifted so that $|1\rangle_j$ and $|0\rangle_{j+1}$ share the same potential and then, after a certain length of time such that $\phi=\pi$, shifted back to its original position; (3) finally a second $\pi/2$-pulse is applied. The resulting logic table is shown in table 1.1.

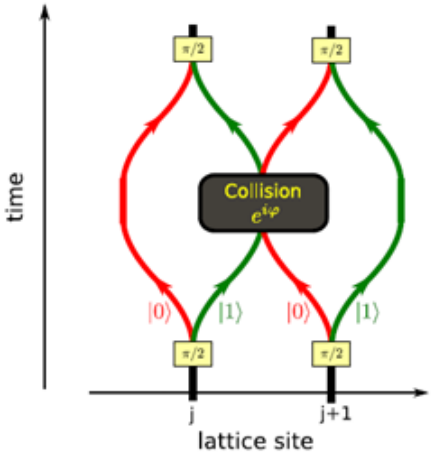

Figure 1.3: Operation of Controlled-NOT (CNOT).

IN $\|\beta_j\rangle\|\beta_{j+1}\rangle$	OUT $\|\beta_j\rangle\|\beta_{j+1}\rangle$
$\|0\rangle\|0\rangle$	$\|0\rangle\|0\rangle$
$\|0\rangle\|1\rangle$	$\|0\rangle\|1\rangle$
$\|1\rangle\|0\rangle$	$-\|1\rangle\|1\rangle$
$\|1\rangle\|1\rangle$	$-\|1\rangle\|0\rangle$

Table 1.1: Logic table of CNOT. NOT works for $|\beta_{j+1}\rangle$ only when $|\beta_j\rangle$ is $|1\rangle$. The minus sign may be eliminated by applying a $3\pi/2$ pulse instead of the second $\pi/2$ puls.

This thesis

In order to perform cold controlled collisions, it is mandatory to have the atoms occupying the motional ground state of the trapping potential in all 3 dimensions. In the donut beam, the mean oscillation number in the radial direction is around $\langle n_{rad} \rangle = 10$. But the same technique used for cooling in axial direction cannot be applied. Therefore, the cooling in radial direction requires Raman cooling. For Raman cooling, we first have to two lasers which have exact desired frequency difference. Such lasers are obtained using a technique called Optical Phase Lock Loop (OPLL). In chapter 2, basic theory of Phase Lock Loop (PLL) which is applicable to OPLL is discussed. Also structure of OPLL and limiting factors occur in OPLL are mentioned in the chapter. In chapter 3, experimental results are presented, and in chapter 4, theory of Raman cooling is discussed.

Chapter 2: Optical Phase Lock Loop

A Phase Lock Loop (PLL) is a feedback control system that forces a local oscillator (LO) to track the frequency and phase of a reference signal within the loop bandwidth. Electronic PLL was first developed more than a half century ago. The same technique for phase locking of lasers is called Optical Phase Lock Loop (OPLL) and is a well established technique in frequency metrology[9] and in cold atoms manipulation[10]. In this chapter, the principle of an OPLL will be presented starting with principle of a PLL, then its application to an OPLL, and finally limitation of the OPLL.

2.1: Phase Lock Loop (PLL)

A schematic of an elementary PLL is shown in figure 2.1. The PLL consists of a Phase Detector (PD), a loop filter, a Voltage-Controlled Oscillator (VCO), and a reference signal. Time-dependent phase of the reference and VCO signals are denoted by $\phi_{\mathrm{Ref}}(t)$ and $\phi_{\mathrm{VCO}}(t)$ respectively. Output voltage of the PD is assumed to be proportional to phase-difference between its input signals:

$$v_{\mathrm{PD}}(t) = K_{\mathrm{PD}} \cdot \left[\phi_{\mathrm{Ref}}(t) - \phi_{\mathrm{VCO}}(t)\right] \tag{2.1}$$

where K_{PD} is the gain factor of the PD.
The output of the PD is fed to VCO through the loop filter, which suppresses noise and high-frequency components and also the filter helps to determine dynamic performance of the PLL. Frequency of the VCO is determined by a control voltage, $v_C(t)$. Deviation of the VCO from its central frequency is $\Delta\omega(t) = K_{\mathrm{VCO}} \cdot v_C(t)$ where K_{VCO} is the gain factor of the VCO. Since frequency is the derivative of phase, the VCO operation is described as $d\phi_{\mathrm{VCO}}(t)/dt = K_{\mathrm{VCO}} \cdot v_C(t)$. By taking Laplace transform of the relation, we obtain

$$L\left[\frac{d\phi_{\mathrm{VCO}}(t)}{dt}\right] = s\phi_{\mathrm{VCO}}(s) = K_{\mathrm{VCO}} \cdot V_C(s). \tag{2.2}$$

Therefore, the phase of the VCO signal is linearly related to the integral of the control voltage:

$$\phi_{\mathrm{VCO}}(s) = \frac{K_{\mathrm{VCO}} V_C(s)}{s}. \tag{2.3}$$

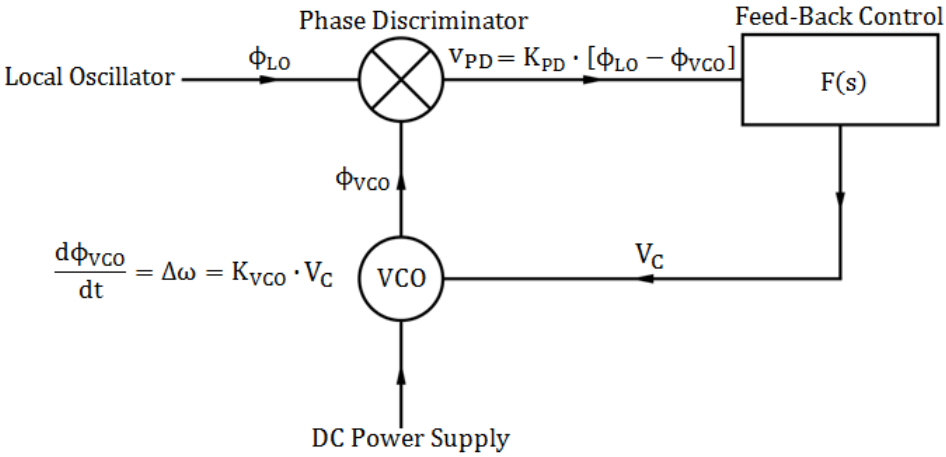

Figure 2.1: Structure of an elementary PLL. Frequency and phase of the VCO track the local oscillator.

One important parameter in analysis of a PLL is the open-loop gain defined as

$$G(s) = \frac{\phi_{VCO,final}(s)}{\phi_{VCO,initial}(s)} = \frac{K_{VCO} \cdot K_{PD} \cdot F(s)}{s}, \tag{2.4}$$

which is the ratio of the VCO phase, $\phi_{VCO,final}(s)$, after one cycle to the initial VCO phase $\phi_{VCO,initial}(s)$. One criterion of a stable PLL is to have the magnitude of the open-loop gain smaller than unity ($|G(s)| < 1$), at the frequency where the phase of the open-loop gain is $-\pi$. When this condition is not satisfied the feed-back loop can oscillate. To observe this condition, a pair of graphs displaying the polar components of G(s), called Bode plot, is often used.
Although a wider loop bandwidth results in a better tracking and acquisition properties, it also contributes to a larger phase jitter due to noise [11]. Therefore, there is always a compromise for between the two for optimum condition.

2.2: Optical Phase Lock Loop (OPLL)

The operation principle of an OPLL is very similar to that of an electronic PLL. Therefore the theoretical analysis of OPLL can be directly borrowed from the theory of PLL. The structure of an OPLL adopted in our experiment is shown in figure 2.2. The purpose of the setup is to phase-lock the slave laser to the master laser so that the frequency difference is exactly a desired frequency around 9.2 GHz. The master and the slave laser beams are overlapped, and the optical signals of the master laser $\sqrt{P_m}\sin(\omega_m t + \phi_m)$ and the slave laser $\sqrt{P_s}\sin(\omega_s t + \phi s$ are combined at a fast photo-diode. The resulting output is

$$P(t) = P_{\approx 9.2GHz} \sin[(\omega_M - \omega_S) \cdot t + (\phi_M - \phi_S)] \tag{2.5}$$

where $P_{\approx 9.2GHz}$ is the power of the beat mode. Higher-frequency components of the beat signal are discarded. In order for us to control the exact frequency difference, the signal frequency is down-converted to around 50 MHz by mixing the signal with a signal from a Phase-Locked Dielectric Resonator Oscillator (PLDRO) with frequency set to 9.15 GHz. In

this frequency range, tunable reference signal is easily provided by a standard signal generator. The down-converted signal is fed to a high-speed comparator along with a reference signal. The comparator compares the error signal (and reference signal) to the ground and produces a digital signal with the error signal (and reference signal) frequency. Then a Phase Frequency Discriminator (PFD) compares the two digital signals and produces output signals based on the phase difference between the two in case the frequency of the two signals are very close and based on the frequency difference otherwise. Of the PFD outputs, one is sent to a PI-control system (called lock-box) which controls a PZT in the slave laser, and one is sent to a loop filter which controls the current modulation signal. The PZT control is used for roughly tracking the master laser frequency and the current modulation control is used for phase-locking. With the two controls, the frequency and the phase of the slave laser is locked to the master laser.

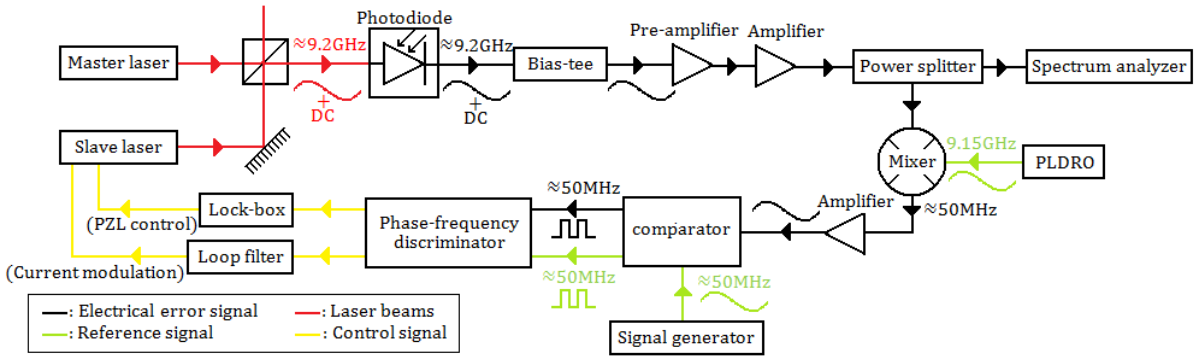

Figure 2.2: Structure of our OPLL setup.

Electric components involved are:

- **Diode lasers (JDSU, SDL-5421-G1)**
  Cavity-extended diode lasers of the same kind are used for both the master and the slave lasers. Wavelength of the lasers are tuned to ≈853nm. Measured linewidth of the lasers is ≈778kHz.
- **Ultra-fast photodiode (Hamamatsu, G4176-03)**
  The ultra-fast photodiode has typical response time of 30ps, effective sensitive area of the photodiode of 0.2mm×0.2mm, typical radiant sensitivity of 0.3A/W at 850nm and maximum incident power of 5mW for CW laser. It requires bias-voltage of 7V for optimal operation.
- **Bias-tee (Mini-circuits, ZX85-12G+)**
  Bias-tee is directly connected to the photodiode as shown in figure 2.3. It provides 7V bias-voltage for the ultra-fast photodiode. Parallel circuit of a 22Ω resistor and a volt-meter are connected between its DC port and a power supply. DC photocurrent of the photodiode is observed by measuring the voltage across the resistor. AC signal detected by the photodiode is taken from RF port.

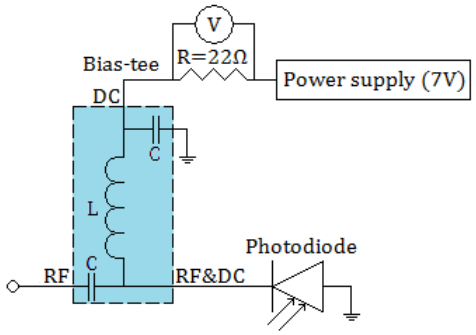

Figure 2.3: Schematics of the bias-tee connected to a power supply and a photodiode.

- **Pre-amplifier (Kuhne Electronics, KU LNA 922 A)**
  The pre-amplifier has gain of ≈25dB at 9.2GHz and bandwidth of ± 10MHz. Amplification of the error signal is required in order to achieve minimum signal power requirement of the ECL comparator.
- **Amplifier (Miteq, AFS5-08001200-40-10P-5)**
  The amplifier has gain of ≈32dB at 9.3GHz and frequency range of 8~12GHz.
- **Power splitter (MCLI, PS2-8)**
  The power splitter has a high frequency range of 8~12.4GHz and a low insertion loss of 0.5dB.
- **Frequency mixer (Mini-circuits, ZMX-10G+)**
- **PLDRO (Resotech, PLDRO-09150-010I)**
  PLDRO produces a reference signal of 9.15GHz. It requires an 10MHz external reference signal with power of 0±4dBm. Its output power is attenuated to 7dBm required by the frequency mixer. In order for stable operation, the 10MHz reference signal power must be kept within the stated range.
- **Amplifier (AU-2A-0150)**
  The amplifier has gain of 32dB and frequency range of 1~500MHz.
- **ECL comparator (Analog Devices, ADCMP563)**
  The dual high speed ECL comparator is used in order to convert error and reference signals to digital signals. It has two different channels for conversion (channel A and B). There are two inputs and two outputs for each channel, one inverting and one non-inverting. Non-inverting Output of a channel is logic high if the analog voltage at the non-inverting input is greater than the analog voltage at the inverting input and vise versa. Non-inverting inputs of both channels are connected to the ground, and the error and the reference signals are fed to inverting inputs. The minimum latch enable differential input voltage is 0.4 V. The HIGH-level output voltage is between -1.15 V and -0.81 V, and the LOW-level output voltage is between -1.95 V and -1.54 V.
- **Phase-frequency discriminator (Analog Devices, AD9901)**
  The key component of the OPLL is a Phase Frequency Discriminator (PFD). The main components of a PFD include four D-flip-flops and an exclusive-OR gate (XOR). PFD operates in two distinct modes: as a linear phase detector and as a frequency discriminator. When the reference and the error signals are very close in frequency, only the phase detection circuit is active. If the two inputs are substantially different in frequency, the frequency discrimination circuit overrides the phase detector portion to

drive the error signal frequency toward the reference frequency and put it within range of the phase detector. Figures 2.4 illustrate the input/output relationships in the phase mode. In the phase mode, only the two input flip-flops and the XOR gate are active. The input flip-flop divides both the reference and oscillator frequencies by a factor of two. This insures that inputs to the XOR are square waves, regardless of the input duty cycles of the frequencies being compared. First each signal goes through a D-flip-flop changing its state at the increasing edges of the signal. Then the resulting signals are sent into a XOR-gate. As seen from the figures 2.4, the resulting output signal has the same frequency as the reference and the oscillator signals, and the average amplitude of the signal is linearly dependent on the phase difference between the reference and the oscillator signal. The output voltage at different oscillation frequency is shown in figure 2.5. In this experiment, the oscillation frequency is chosen to be around 50 MHz. A parallel resistance of 182 Ω is connected to the inverting-output of the PFD as a standard application of the component providing $K_{PFD} \approx -0.285\ V/rad$. For the non-inverting-output, no parallel resistance is added providing $K_{PFD} \approx -1.5\ mA/rad$. The inverting-output provides voltage signal for the PZT control and the non-inverting-output provides current signal for the current modulation control.

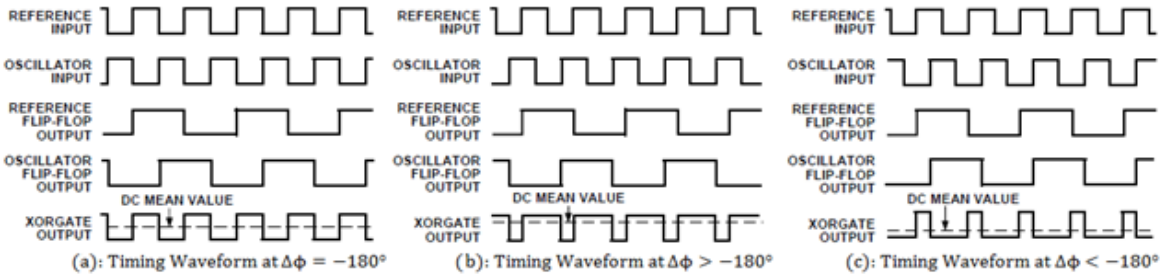

Figure 2.4: Input/ output signals of PFD. DC mean value of the output is linearly dependent on the phase difference.

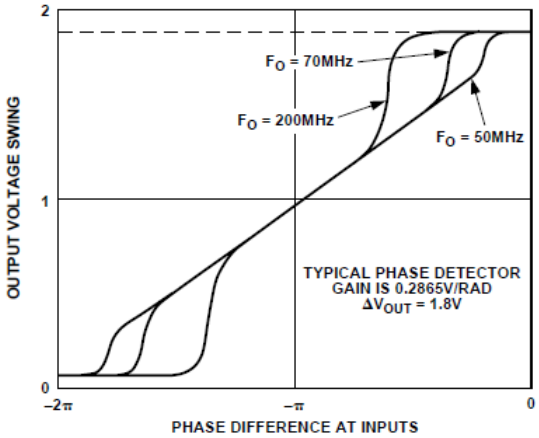

Figure 2.5: Output voltage of PFD in phase mode. At signal frequency of 50 MHz, the PFD has maximum linear operation range.

– **Lock-loop filter**

A lock-loop filter is connected between the non-inverting-output and the modulation-current input of the slave-laser. The purpose of this lock-loop filter is to compensate for the phase-delay of the error signal occurs in the process of the OPLL as well as to suppress noise signal. The structure of the lock-loop filter is shown in figure 2.6. The lock-loop filter mainly consists of three pars:

1. Low-pass filter: A simple RC-low-pass filter is used to suppress high frequency component of the error signal.
2. Modified high-pass filter: A modified high-pass filter is used for induce the phase advance to counter the phase delay. In addition to the standard RC-high-pass filter, a potentiometer is connected parallel to the capacitor in order to be able to control the phase advance.
3. Amplitude controller: A potentiometer is used to further reduce the amplitude of the error signal.

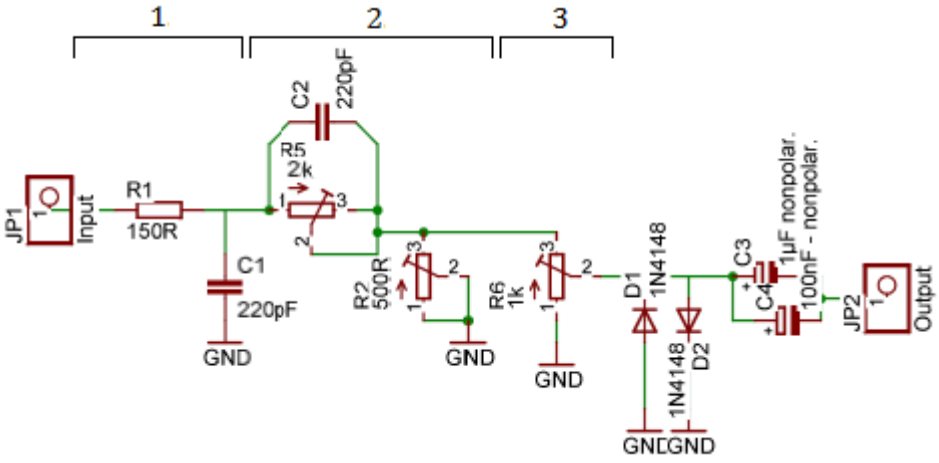

Figure 2.6: Structure of lock-loop filter.

2.3: Limiting Factors of the OPLL

In the proposed OPLL, there are two factors which limit the bandwidth of the system. The limiting factors are:

– **The Transfer Function of the Laser Diode**

Though in the electrical PLL explained above, the response of the VCO is assumed identical for the range of the modulation frequency, this is not the case for the laser diode. The FM response of a laser stems from two opposite contributions, thermal response and carrier density response. The thermal response is effective at low frequency, while the carrier density FM response is constant from DC to the relaxation frequency.

In one-dimensional model, the thermal contribution to the FM response [12] is given by

$$H_{th}(s) = -K_{th}\frac{\tanh\left(\sqrt{\frac{s}{f_c}}\right)+\tanh\left(\frac{\sqrt{s}}{2\sqrt{f_c}}\right)}{\sqrt{\frac{s}{f_c}}},$$

where K_{th} is a factor which depends on parameters of the laser, s is the Laplace variable, f_c is the thermal cut-off frequency.

At low frequency, the carrier density FM response, H_{el}, response is considered constant and in phase with the current.

The total FM response is given by adding the two contributions,

$$H_{FM}(s) = H_{el} - K_{th} \frac{\tanh\left(\sqrt{\frac{s}{f_c}}\right) + \tanh\left(\frac{\sqrt{s}}{2f_c}\right)}{\sqrt{\frac{s}{f_c}}}.$$

– **Delay of the control signal**

In a control system, there always exists phase delay of control signal due to its traveling time. In OPLL, the delay is due to traveling time of the laser beam from the slave laser to the photodiode and traveling time of the electric signal from the photodiode to the current modulation input of the slave laser. The distance between the slave laser to the photodiode is around 1.13 m, and the length of the SMA and BNC cables between the photodiode and the slave laser is around 1.56 m. Assuming the speed of electric signal to be around 2/3 of the speed of light, the combined traveling time of the control signal is estimated to be around 16 ns. The resulting phase delay of the control signal contributes to the open loop gain:

$$G'(s) = G(s) \cdot e^{-i \cdot s \cdot \tau_{delay}} = \frac{K_{VCO} \cdot K_{PD} \cdot F(s) \cdot e^{-i \cdot s \cdot \tau_{delay}}}{s},$$

where τ_{delay} is the combined delay time.

Chapter 3: Experimental Study and Realization of OPLL

In constructing the setup for OPLL, progress was made in backward. First, the OPLL setup was constructed, and then measurement of FM response of the slave laser was performed. With the knowledge of the FM response, study and optimization of OPLL was then attempted. However, a miscalculation was made in estimation of the FM response which caused discrepancy between expected and observed behavior. For this reason, though apparent phase-lock was established and measurements were made, the behavior of the OPLL was completely unexpected and the fact that the control signal was severely weak was not identified in time. The miscalculation was identified about a week ago and the result indicates the observed behavior of OPLL appropriately. The following analysis was made with the result.

3. 1: Measurement of the FM response

In the previous chapter, the modulation-frequency dependent FM response of laser diode was mentioned. The FM response of the slave laser was measured using a Michelson interferometer as shown in figure 3.1. The optical length difference is set around 1 cm and the optical power of arm 1 and 2 are measured to be 0.5 mW and 0.3 mW respectively. Modulation current was provided by a network analyzer (Agilent, N9010A), and the resulting signal from the Michelson Interferometer was detected by a fast-photodiode (Thorlabs, DET10A) and analyzed by the network analyzer. Power of the modulation current was set to be -50 dBm. During the measurement, the slave laser was locked to the master laser using only PZT control, and the master laser was locked to a cavity for stability. The frequency of the master laser was tuned such that the frequency of the slave laser lay around the centre frequency of the interferometer as shown in figure 3.2. As the modulation current is applied, the frequency of the slave laser oscillates producing optical intensity at the photodiode oscillating at the same frequency as the modulation current. From the amplitude of the oscillation, the FM response of the slave laser was determined. Also intensity modulation due to the current modulation was measured by blocking one arm of the interferometer.

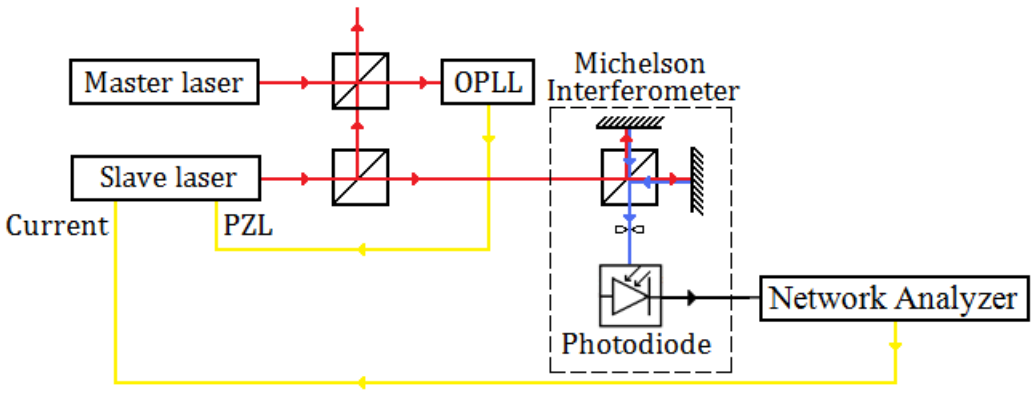

Figure 3.1: Michelson interferometer setup for measuring FM response of the slave laser. The slave laser is locked to the master laser with PZT control. Network analyzer provides the modulation current and analyzes the resulting signal.

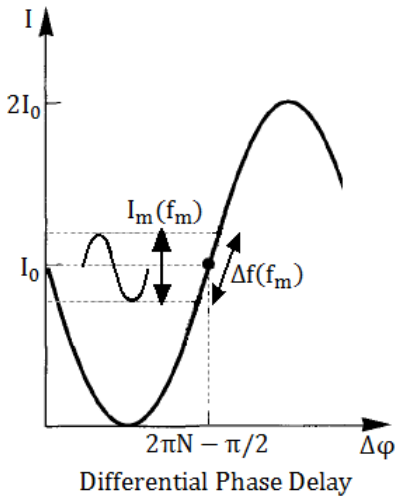

Figure 3.2: Michelson interferometer signal. As the frequency of the slave laser oscillates at the frequency of the modulation current, the resulting signal of the Michelson interferometer also oscillates at the frequency.

The measured FM and IM responses of the slave laser are shown in figure 3.3. The measured intensity modulation signal and the measured frequency modulation signal are given by

$$\mathrm{IM_{Measured}[W]} = \frac{(\mathrm{APD[A/W]\cdot AMP[V/A]\cdot IM[W/A]\cdot I[A]})^2}{\mathrm{R[\Omega]}} \tag{3.1}$$

$$\mathrm{FM_{Measured}[W]} = \frac{(\mathrm{APD[A/W]\cdot AMP[V/A]\cdot\{MI[W/Hz]\cdot FM[Hz/A]+k\cdot IM[W/Hz]\}\cdot I[A]})^2}{\mathrm{R[\Omega]}} \tag{3.2}$$

where MI is the slope of the Michelson interferometer signal around the centre, APD is the optical intensity to the photocurrent ratio of the photodiode, AMP is the gain of the photodiode, FM is the frequency modulation response of the slave laser to the applied modulation current, I is the applied modulation current, R is the input resistance of the network analyzer, IM is the intensity modulation response of the slave laser, and k is the contribution factor of IM. Therefore, the FM is given by

$$\mathrm{FM} = \frac{\sqrt{\mathrm{FM_{Measured}\cdot R}} - \mathrm{k_1}\cdot\sqrt{\mathrm{IM_1\cdot R}} - \mathrm{k_2}\cdot\sqrt{\mathrm{IM_2\cdot R}}}{\mathrm{APD\cdot MI\cdot AMP\cdot I}} \tag{3.3}$$

where 1 and 2 denotes IM contribution from arm 1 and 2. The estimated values of the parameters are APD=0.35 A/W, AMP=5 kV/A, MI≈1.29×10^{-14} W/Hz, R=1 MΩ, and I=50 μA. $k_{1,2}$ are estimated to give the best fitting result. The result of least-square-root fitting is shown in figure 3.4. As mentioned in the previous chapter, the FM response is given by

$$\mathrm{H_{FM}}(s) = \mathrm{H_{el}} - \mathrm{K_{th}}\frac{\tanh\left(\sqrt{\frac{s}{f_c}}\right)+\tanh\left(\frac{\sqrt{s}}{2f_c}\right)}{\sqrt{\frac{s}{f_c}}}. \tag{2.4}$$

The estimated values of the parameters are $\mathrm{H_{el}} = 3.2 \times 10^5 \pm 0.3 \times 10^5$ Hz/A, $\mathrm{K_{th}} = 3.6 \times 10^5 \pm 0.2 \times 10^5$ Hz/A, and $f_c = 1.6 \pm 1.2$ MHz.

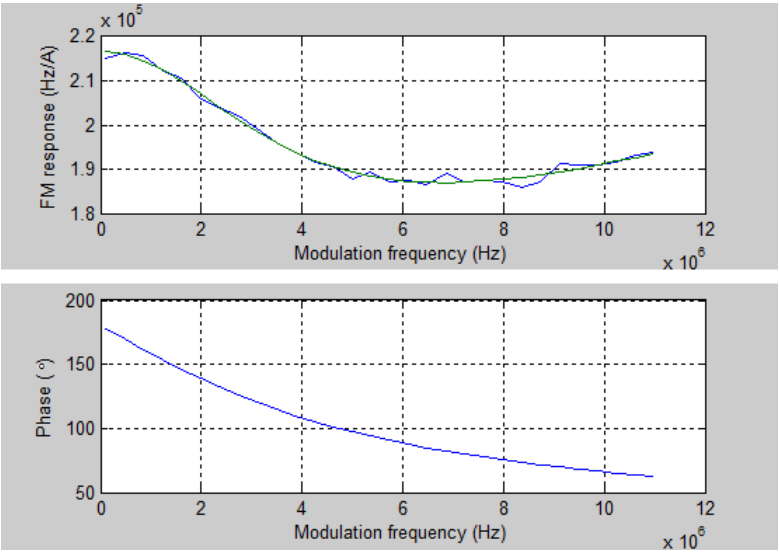

Figure 3.4: Measurement (blue line) and theoretical fitting (green line) of the FM response of the slave laser.

3.2: Estimated open-loop gain and Bode plot

With the estimated FM response of the slave laser, the open-loop gain is evaluated and Bode plot is drawn in order to identify the optimal condition of OPLL. Bode plots of various loop-filter settings are shown in figures 3.6 and 3.7. Figures 3.6 show phase of open-loop gain, and figures 3.7 show magnitude of open-loop gain. In both figures, three plots of different R3 values are shown, and in each plot six lines with different R2 values are drawn. In all cases the potentiometer in the section 3 of the loop-filter mentioned above is set to minimum in order to have the maximum error signal amplitude. Figures 3.6 suggest that a lower R3 results in a higher –π-frequency and that in case of a high R3, a lower R2 results in a higher –π-frequency. However, figures 3.7 suggest that at a low R2, the magnitude of open-loop gain is too low to achieve OPLL. Also a simulation shows that the maximum magnitude of open-loop gain at –π-frequency cannot be larger than -1 dB with our current setup. Therefore, the optimal condition for OPLL is achieved by setting R2 to minimum and tuning R3 such that the error signal amplitude and the bandwidth of the loop are balanced.

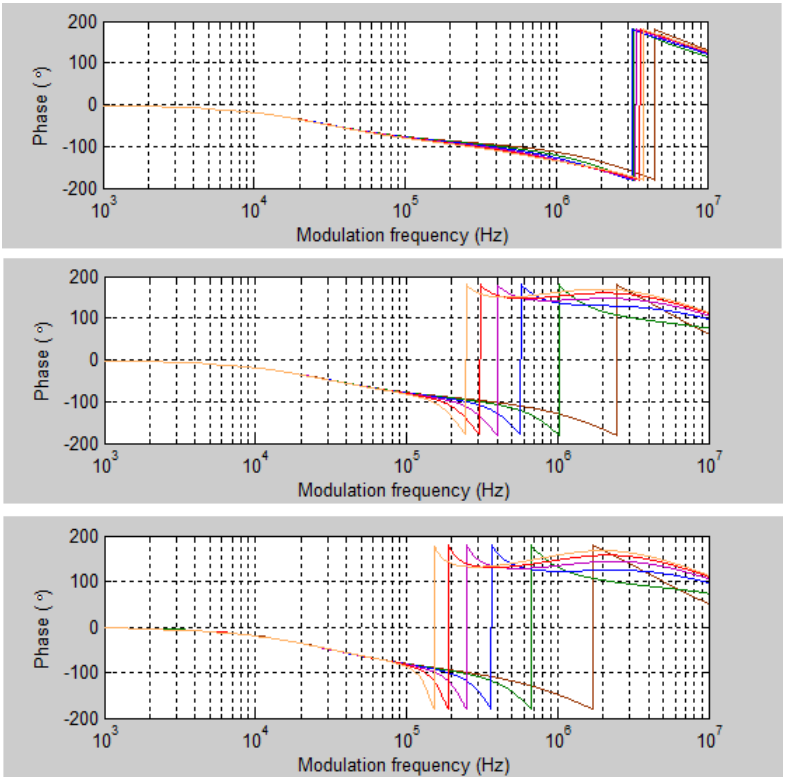

Figures 3.6: Phase of open-loop gain. (top) R3=1, (middle) R3=300, (bottom) R3=500. From brown to orange lines, values of R2 are increased from 1 to 2k ohm. As R3 is increased the bandwidth become narrower, and to keep the bandwidth as wide as possible R2 needs to be kept minimum.

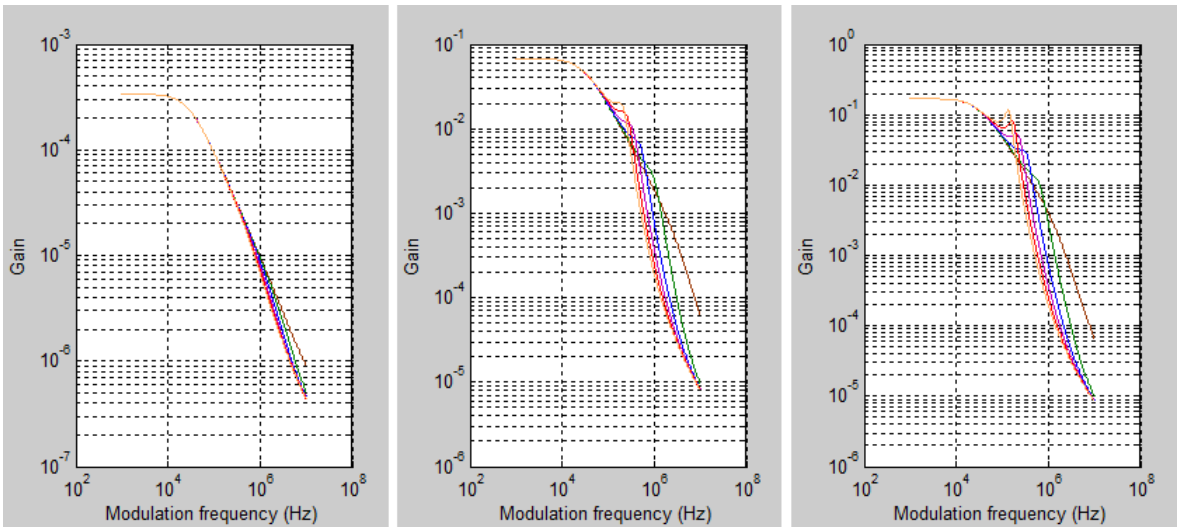

Figures 3.7: Gain of open-loop gain. (left) R3=1, (centre) R3=300, (right) R3=500. From brown to orange lines, values of R2 are increased from 1 to 2k ohm. In order to have sufficiently high gain, R3 needs to be set sufficiently high.

3.4: Realization of OPLL

According to the open-loop gain obtained above, the optimization of OPLL was attempted. The beat signal observed under the best condition is shown in figures 3.8. The condition under which these data were obtained is R2≈1Ω, R3≈426Ω with the amplitude control set to maximum. Figure 3.8 (a) shows the beat signal with the frequency range of 1GHz spanned around the centre frequency of 9.2GHz. It shows the sidebands separated by 50MHz from each other which is caused by the 50MHz control signal. Figure 3.8 (b) shows the signal with the range of 10MHz. It shows servo bumps at around 500kHz away from the centre frequency due to narrow bandwidth of the condition. Figure 3.8 (c) spans the range of 10kHz and shows sidebands. Result of analysis suggests that the peaks are not caused by phase noise in any signal source including the lasers as there exists no peak in spectral density of phase error caused by noise. Also measurements taken with different control signal amplitude shown in figure 3.9 exhibits increase in sidebands amplitude when control signal amplitude is reduced slightly which is the opposite behavior to be expected. And reduction in sidebands amplitude was observed when proportional-factor of the lock-box was reduced. Figure 3.8 (d) shows the signal with the range of 20Hz. From this plot, we see that the linewidth of the beat signal is at least 2Hz which is the minimum resolution of the spectrum analyzer. Of the energy distributed between $\pm$10 MHz, ≈94% is contained within the peak.

Though the estimated 94% of the energy is stored in the carrier, improvements have to be made to study and improve the quality of OPLL. The most important improvement to be made is to amplify the control signal from PFD. Bode-plot and experimental results suggest that currently the control signal is severely weak. This improvement will allow separate control of control signal amplitude and loop bandwidth and will result in a wider bandwidth.

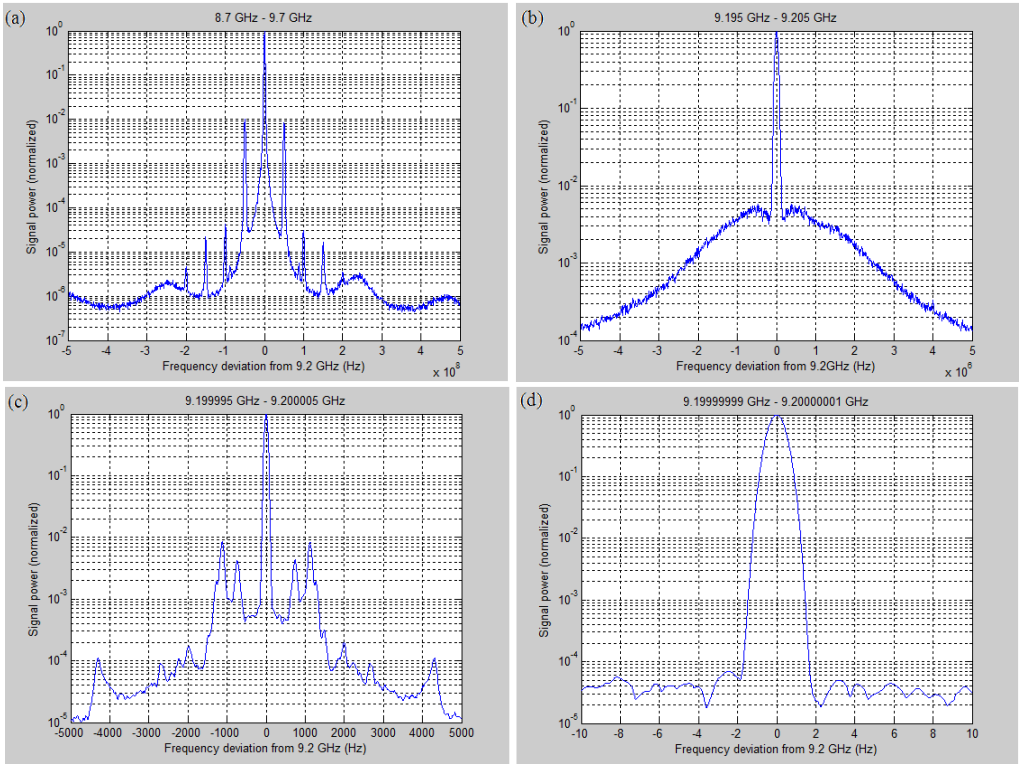

Figures 3.8: Spectrum of beat signal. (a) 8.7GHz-9.7GHz, (b) 9.195GHz–9.205GHz, (c) 9.199995GHz-9.200005GHz, (d) 9.19999999 GHz-9.20000001GHz

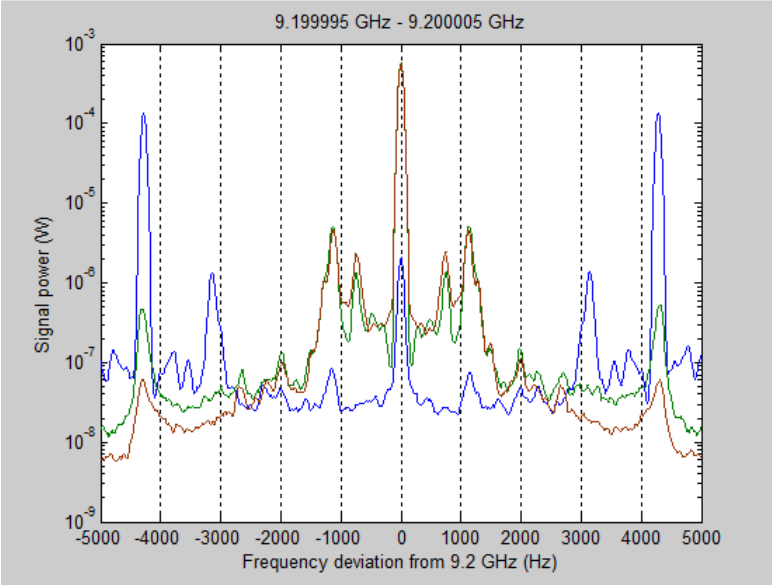

Figure 3.9: Measurement of the beat signal with different the control signal amplitude. The brown line is measured with the highest amplitude while the blue line is measured with the amplitude 15% less than the maximum. Growing of the sidebands is not expected if they are caused by phase noise of signal sources.

Chapter 4: Theory of Raman Cooling and Outlook

In our group, we use neutral Cesium atoms as qubits that are stored in |0⟩=|F=4,m=4⟩ and |1⟩=|F=3,m=3⟩. The atoms are trapped in 1D optical lattice and are expected to be further trapped in radial direction by a donut-mode laser. In order to demonstrate entanglement of the atoms, cooling of the atoms to the motional ground state in 3D is required. The cooling in 1D along the optical lattice has already been achieved by sideband cooling. Though improvement of the OPLL is possible, OPLL technique demonstrated locking of a laser to another laser with tunable exact frequency difference. The tunable exact frequency difference is the key to demonstrating Raman-cooling.

4.1 Raman-Transition

Raman-Transition is a coherent population transfer method which involves two lasers called pump and Stokes laser and an atom with three energy levels in Λ-configuration as shown in figure 4.1. The pump and the Stokes lasers are characterized by the frequency $\omega_{P,S}$ and Rabi frequency $\Omega_{P,S}$. The frequency of the pump and the Stokes lasers are detuned from the resonance frequencies, $\Delta E_{12} = E_2 - E_1$ and $\Delta E_{23} = E_2 - E_3$, by a large detuning of Δ in order to avoid excitation to the excited state $|2\rangle$. δ in figure 4.1 represents the detuning from the two-photon resonance ($\omega_P = \omega_S + \Delta_{HFS}$).

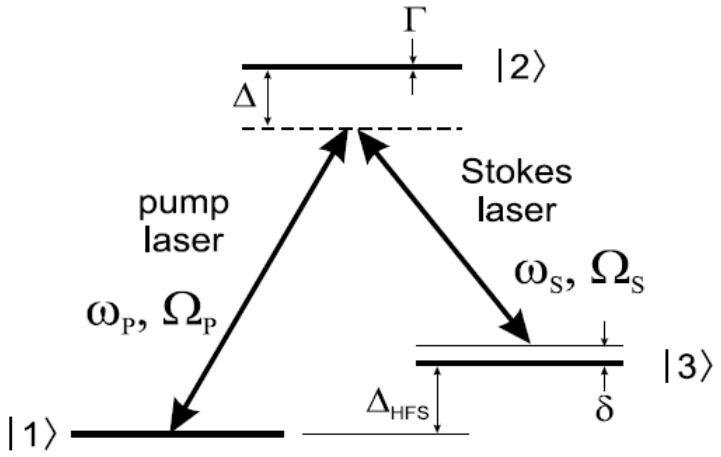

Figure 4.1: Three-level atom in Λ-configuration for Raman-transition

The wavefunction of the system at a time t, Ψ(t), is expressed as a superposition of the bare states |1⟩, |2⟩ and |3⟩:

$$\Psi(t) = C_1(t) \cdot |1\rangle + C_2(t) \cdot |2\rangle + C_3(t) \cdot |3\rangle, \tag{4.1}$$

where the coefficients $C_i(t)$ is the probability amplitudes.

The Hamiltonian, which describes the coupling of the three states by two coherent radiation fields within the rotating wave approximation (RWA), reads

$$\hat{H} = \frac{\hbar}{2}\begin{bmatrix} 0 & \Omega_P & 0 \\ \Omega_P & 2\Delta & \Omega_S \\ 0 & \Omega_S & 2\delta \end{bmatrix}. \tag{4.2}$$

The Rabi frequencies $\Omega_{P,S}$ are defined as

$$\Omega_{P,S} = -\frac{\hat{\mathbf{d}}\cdot\mathbf{E}}{\hbar} = \Gamma\sqrt{\frac{I}{2I_0}}. \tag{4.3}$$

Here Γ is the linewidth of the excited level, I is the laser intensity, and I_0 is the saturation intensity.

Using (4.1) and (4.2) in the time-dependent Schrödinger equation, we obtain a set of linear differential equations for the probability amplitudes C_i:

$$\begin{cases} i\dot{C_1} = \frac{1}{2}\Omega_P C_2 \\ i\dot{C_2} = \frac{1}{2}\Omega_P C_1 + \Delta C_2 + \frac{1}{2}\Omega_S C_3 \\ i\dot{C_3} = \frac{1}{2}\Omega_S C_2 + \delta C_3. \end{cases} \tag{4.4}$$

With the adiabatic elimination, the three-level system reduces to an effective two-level system:

$$\begin{cases} i\dot{C_1} = \frac{\Omega_P}{4\Delta}(\Omega_P C_1 + \Omega_S C_3) \\ i\dot{C_3} = -\delta C_3 + \frac{\Omega_S}{4\Delta}(\Omega_P C_1 + \Omega_S C_3), \end{cases} \tag{4.5}$$

with the new Hamiltonian:

$$\hat{H}_{eff} = \frac{1}{4}\begin{pmatrix} \frac{\Omega_P^2}{\Delta} & \frac{\Omega_P\Omega_S}{\Delta} \\ \frac{\Omega_P\Omega_S}{\Delta} & \frac{\Omega_S^2}{\Delta} - 4\delta \end{pmatrix}. \tag{4.6}$$

Solving (4.5) and assuming that initially an atom is in state $|1\rangle$, the time dependence of the state populations is given as

$$\begin{cases} |C_1|^2 = 1 - \Lambda \cdot sin^2\left(\frac{\Omega_0}{2}t\right) \\ |C_3|^2 = \Lambda \cdot sin^2\left(\frac{\Omega_0}{2}t\right), \end{cases} \tag{4.7}$$

where $\Lambda = \Omega_R^2/\Omega_0^2$ is the amplitude of the population oscillation, $\Omega_0 = \sqrt{\Omega_R^2 + \delta^2}$ is the generalized Rabi frequency and Ω_R is the resonance Rabi frequency at which the atomic population oscillates between these states when the Raman transition is resonant

$$\Omega_R = \frac{\Omega_P\Omega_S}{2\Delta}. \tag{4.8}$$

From Eq. 4.7, we see that the population oscillates between state |1⟩ and state |3⟩ and a complete population transfer from state |1⟩ to state |3⟩ can be achieved when the two-photon resonance is established and when we apply the two lasers for an amount of time $t' = \pi/2\Omega_0$.

It is important to note that, despite the large detuning Δ, it is possible for the atoms to be excited to the excited level. For a large detuning, the scattering rate is given by

$$\Gamma_{SC} = \frac{\Gamma}{2}\frac{I}{I_0}\left(\frac{\Gamma}{2\Delta}\right)^2. \tag{4.9}$$

As the scattering rate is proportional to Δ^{-2} and the Rabi frequency is proportional to Δ^{-1}, we need to find a compromise between the desired reduction of the scattering rate and the unwanted reduction of the Rabi frequency.

4.2: Raman-Transition with a Cesium Atom

In our experiment, we manipulate cesium atoms using the D_2-transition at 852nm between the $6S_{1/2}$ and $6P_{3/2}$ states. The ground state is split into two hyperfine states |F=3⟩ and |F=4⟩ due to hyperfine interaction. The energy difference between the two ground states is Δ_{HFS}=2π·9.19263177 GHz. The excited state has the linewidth of Γ=2π·5.22 MHz. Cesium atoms are laser-cooled to the temperature of around 10 μK and then loaded to 1D-optical lattice. A magnetic field of 3G is applied along the axis of the lattice in order to define the quantization axis. Atoms are stored in the states |F=3, m_F=3⟩ and |F=4, m_F=4⟩ by using σ^+-polarized optical pumping lasers. Due to the magnetic field applied, the energy difference between the ground states are reduced by 2π·1.062 MHz. |F=4⟩ is chosen as the initial state as it is the dark state.

The spin orientation of cesium atom and the polarization of the pump and the Stokes laser affect the dipole moment, and the resulting Rabi frequency is given by

$$\Omega'_R = \Omega_R\sqrt{X(m_F)}, \tag{4.10}$$

where the coefficient X(m_F) is given by [13]

$$X(m_F) = \begin{cases} \frac{1}{288}(4+m_F)(5+m_F) : (\pi,\sigma^-),(\sigma^+,\pi) \\ \frac{1}{288}(4-m_F)(5-m_F) : (\pi,\sigma^+),(\sigma^-,\pi) \\ \frac{1}{9}\left[1-\left(\frac{m_F}{4}\right)^2\right] : (\sigma^+,\sigma^+),(\sigma^-,\sigma^-) \\ 0 : (\pi,\pi),(\sigma^\pm,\sigma^\mp) \end{cases}. \tag{4.11}$$

4.3: Raman-Cooling

For an atom trapped in a harmonic potential, there exist discrete motional states |n⟩ with energies

$$E_n = \left(n + \frac{1}{2}\right)\hbar\omega_{\mathrm{rad}} \tag{4.12}$$

where ω_{rad} is the oscillation frequency in the radial direction as shown in figure 4.2. reducing the frequency of the Stokes laser by $\hbar\omega_{\mathrm{rad}}$, Raman-transition transfers an atom from state |1,n⟩ to |3,m=n-1⟩ reducing the motional quantum number by 1. Once the atom is in |3, n-1⟩, the optical pumping lasers are applied which brings the atom into |1⟩. During the optical pumping, the transition rate for transitions |n⟩→|n±1⟩ are given by [14]

$$\gamma_{n\to n+1} = A_+ \cdot (n+1), \tag{4.13. a}$$

$$\gamma_{n\to n-1} = A_- \cdot n, \tag{4.13. b}$$

where $A_\pm$ are the coefficients which in the case of the optical pumping have the same value as shown in figure 4.3. As the transitions |n⟩↔|n+1⟩ (|n⟩↔|n-1⟩) have the same transition rate $A_+ \cdot (n+1)$ ($A_- \cdot n$), the overall oscillatory state remain the same after the optical pumping. By repeating this process, the atom will be cooled to the ground state of the motional states. When the atom is in the ground state of the oscillatory states, the atom will be in dark state as there is no lower oscillatory state.

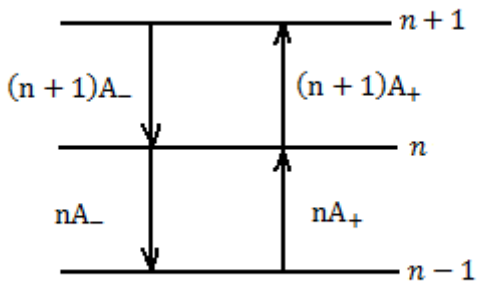

Figure 4.2: Transition rates from and to the oscillatory state n. $A_\pm$ are the coefficients which in the case of the optical pumping have the same value [14].

The dependence of the Rabi-frequency on the motional state is given by [15]

$$A_{n\to m} = \left|\langle m|e^{i\Delta\mathbf{k}\hat{z}}|n\rangle\right| = \left|e^{-\frac{1}{2}(\Delta k z_0)^2}(n!\,m!)^{1/2}(i\Delta k z_0)^{\Delta n}\sum_{l=0}^{n_<}\frac{(-1)^l(\Delta k z_0)^{2l}}{l!(l+\Delta n)!(n_<-l)!}\right| \tag{4.14}$$

where z_0 is the spread of the wave function of the oscillatory ground state, $\Delta\mathbf{k} = \mathbf{k}_\mathrm{p} - \mathbf{k}_\mathrm{s}$ is the difference in the wave vector between the pump and the Stokes laser, $\Delta n = n - m$, and $n_<$ is the lesser of n and m.

The resulting Rabi frequency is given by

$$\Omega_{n\to n-1} = A_{n\to n-1} \cdot \Omega'_\mathrm{R}. \tag{4.15}$$

There are several conditions for Raman-cooling:

1. Lamb-Dicke condition, $\eta = \hbar k^2/2m\omega_{rad} \ll 1$, has to be satisfied for both the pump and the Stokes lasers. η is the ratio of the amplitude of the zero-point motion of the trapped atom to the wavelength of the lasers.
2. The propagation direction of the pump and the Stokes lasers needs to be opposite to each other. This is because the change in the oscillatory state requires momentum change, and momentum transfer from the laser beams is the highest under this condition. This effect can be also seen in the transition probability which is proportional to Δk [14].
3. For Raman-transition to happen primarily with the change of the oscillatory quantum number Δn=-1, $\Omega_{n\to n-1} \ll \omega_{rad}$ has to be satisfied. This is because according to eq. (4.7), $\Lambda = (\Omega_{n\to n-1}/\Omega_0)^2$ with $\Omega_0 = \sqrt{\Omega_{n\to n-1}^2 + \delta^2}$, and assuming that the two-photon detuning δ=0 but replacing it with ω_{rad} for transition with Δn=+1 (or -2), suppression of the undesired transition requires $\Lambda \ll 1$, and therefore, Δn=-1.

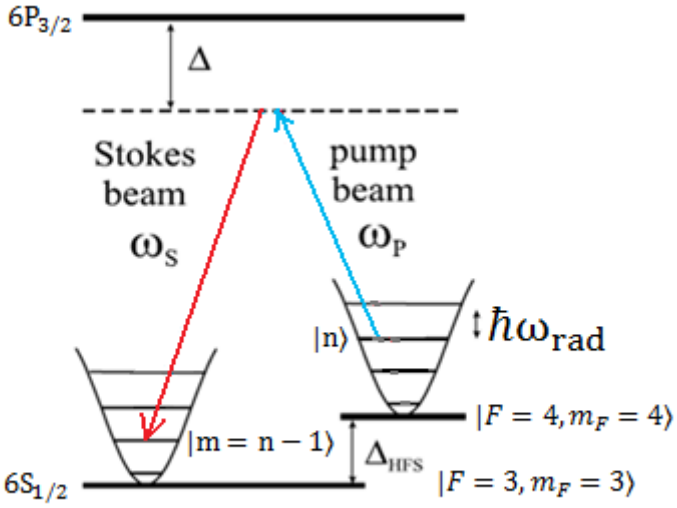

Figure 4.3: Raman-cooling scheme. $|F = 4, m_F = 4\rangle$ is the initial state, and the atom is Raman transferred to $|F = 3, m_F = 3\rangle$.

4.4: Measurement of Oscillatory State

As it was mentioned previously, the transition rate for transitions $|n\rangle \to |n\pm1\rangle$ during the optical pumping are given by eqs. (4.13). As the intensity of the scattered light is proportional to the transition rate,

$$I_{red} \propto \gamma_{n+1} \text{ and} \tag{4.16. a}$$

$$I_{blue} \propto \gamma_{n-1}, \tag{4.16. b}$$

the measurement of the red- and blue-detuned scatted light intensity can be used to determine the oscillatory state of the atom,

$$\langle n \rangle = \frac{I_{blue}}{I_{red} - I_{blue}}. \tag{4.17}$$

4.5: Experimental Setup

In our experimental setup, we plan to direct the Raman lasers to atoms by the same way we apply the MOT laser as shown in figure 4.4. The pump and the Stokes lasers are σ^+-polarized. As the laser beams are not parallel to the quantization axis, the polarization of the light is taken as ($\sigma^{\pm}$, π) for the Raman lasers incident on the atoms vertically (hereafter called "vertical lasers"), (σ^+, π) for the incoming Raman lasers incident on the atoms horizontally (hereafter called "horizontal lasers") and (σ^-, π) for the reflected horizontal lasers, and geometrical factors have to be taken into account when calculating Rabi-frequency. The geometrical factor is $(1/\sqrt{2})$ for π-polarization and (1/2) for $\sigma^{\pm}$-polarization for vertical lasers and $(\sqrt{2/3})$ for $\sigma^{+,-}$-polarization and $(\sqrt{1/3})$ for π-polarization for horizontal lasers. As it was mentioned previously, the combination of polarization for the pump and the Stokes laser plays important role. The possible combinations are $(\pi,\sigma^+),(\pi,\sigma^-),(\sigma^+,\pi),(\sigma^+,\sigma^+),(\sigma^-,\pi),(\sigma^-,\sigma^-)$ and, for horizontal lasers, there are 20 possible combinations and, for vertical lasers, there are 8 possible combinations. These combinations result in different Rabi-frequencies and the resulting Rabi-frequency is the sum of all of the Rabi frequencies.

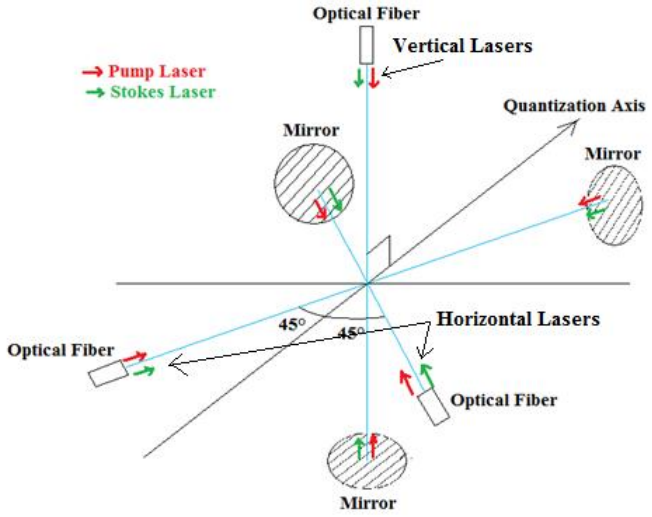

Figure 4.4: Experimental setup of Raman-cooling. As the pump and the Stokes lasers are not parallel to the quantization axis, σ^+-polarization of the lasers are seen as the mixture of $\sigma^{\pm}$- and π-polarizations.

4.6: Simulation and analysis

According to the Boltzmann distribution, for the temperature of 10 μK, the oscillation frequency of $2\pi\cdot 20$ kHz, the average oscillation quantum number is 10, and the occupation probability of the oscillatory states are shown in Figure 4.5.

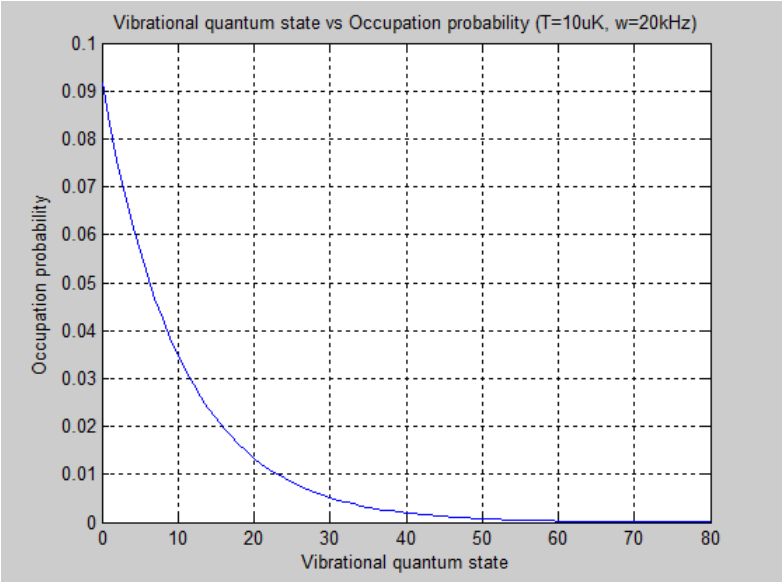

Figure 4.5: Distribution of motional energy states.

Horizontal Lasers

The second condition for Raman-cooling is satisfied for both the pump and the Stokes lasers with $\frac{\hbar {k_P}^2}{2m\Omega_z} = \frac{\hbar {k_S}^2}{2m\Omega_z} = 0.23$. Figure 4.6 shows the oscillatory state dependence of Rabi-frequency. It predicts that there are minimum and maximum values. The maximum values occur at n=7 and at n=37, and the minimum values occur at n=18 and at n=60. Figure 4.7 shows the dependence of $\Omega_{n\to n-1}$ on the detuning for the oscillatory state of |n=37⟩. The oscillatory state was chosen as it exhibits the highest Rabi frequency according to Figure 4.6. From the figure, we see that in order to satisfy the third condition of Raman-cooling, the detuning should be greater than at least 100 GHz. Figure 4.8 shows the Rabi-transition from the initial oscillatory states for the intensity of the Raman-lasers of 1 mW. In order for Raman-cooling, we need to apply optical pumping lasers after some time. As the Rabi-frequency depends on the initial oscillatory states, this timing for the optical pumping lasers cannot be set at an ideal time for every oscillatory state. The timing is determined by the highest Rabi-frequency among the oscillatory states of interest. From the picture, the appropriate time would be 0.8 ms in this case. In the time, in some states, more than 90% of population transfer is achieved, while in other states, the population transfer is less than 1%. The smallest fraction of population transfer occurs for the states |n=18⟩ and |n=60⟩ with 0.08% and 0.3% population transfer respectively. Though the probability of population transfer for those states are very small, the atoms in those states still should undergo Raman-cooling within a second.

Vertical Lasers

The first condition for Raman-cooling is satisfied for vertical lasers with $\frac{\hbar {k_P}^2}{2m\Omega_z} = \frac{\hbar {k_S}^2}{2m\Omega_z} = 0.31$. As it is the case for the horizontal lasers, Rabi-frequency, $\Omega_{n\to n-1}$, for vertical lasers also varies with oscillatory states as shown in figure 4.9. Figure 4.10 shows the relation between Rabi-frequency and the detuning for the initial motional states |n=45⟩ which exhibits the

highest Rabi-frequency for the intensity of the pump and the Stokes laser of 2 mW. From the figure, we see that the third condition, $\Omega_{n\to n-1} \ll \omega_{rad}$, is satisfied for the detuning larger than 50 GHz. Figure 4.11 shows Rabi-frequency for different initial oscillatory state. From figure 4.11, we see that the timing of the optical pumping lasers should be around 2 ms. For this, 0.02% of the atoms in $|n=9\rangle$ and 0.054% of the atoms in $|n=30\rangle$ are expected to undergo Raman-cooling. Therefore, we expect these states to be cooled within 10 seconds.

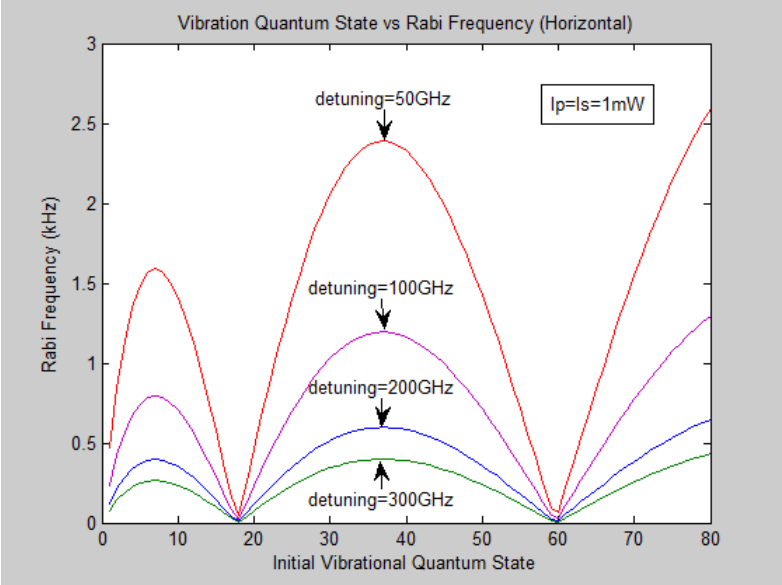

Figure 4.6: Dependence of Rabi frequency on oscillatory state for different detuning. The predicted Rabi frequency varies with oscillatory state. There are oscillatory states which experience maximum and minimum Rabi frequencies.

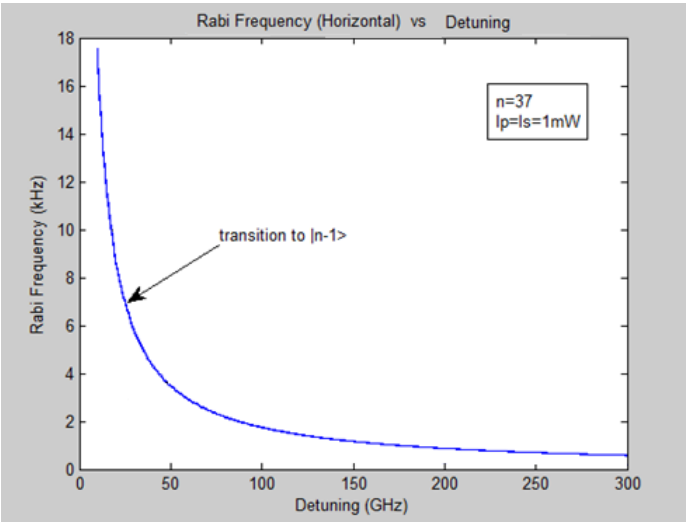

Figure 4.7: Dependence of Rabi frequency, $\Omega_{n\to n-1}$, on the detuning. The third condition of Raman-cooling requires that $\Omega_{n\to n-1} \ll \omega_{rad} \approx 2\pi \cdot 20$ kHz. For this the detuning should be greater than at least 100 GHz.

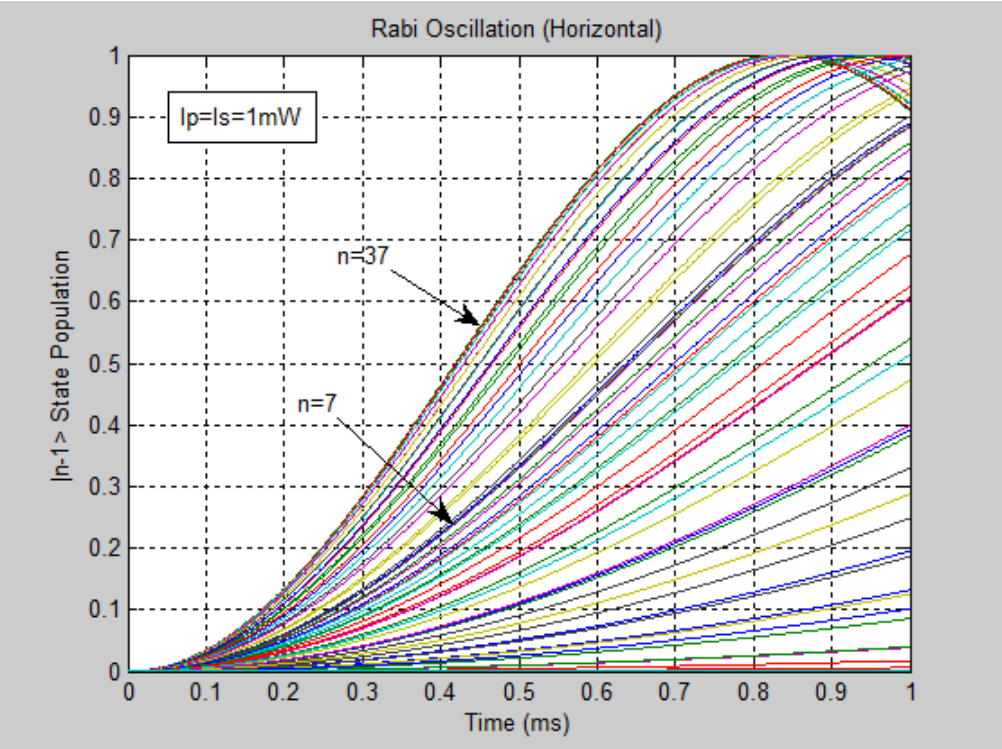

Figure 4.8: Rabi-oscillation for different initial oscillatory states. As Rabi-frequency varies with the oscillatory states, the timing of the optical pumping lasers has to be determined with the highest Rabi-frequency. In this case, the timing should be around 0.8 ms.

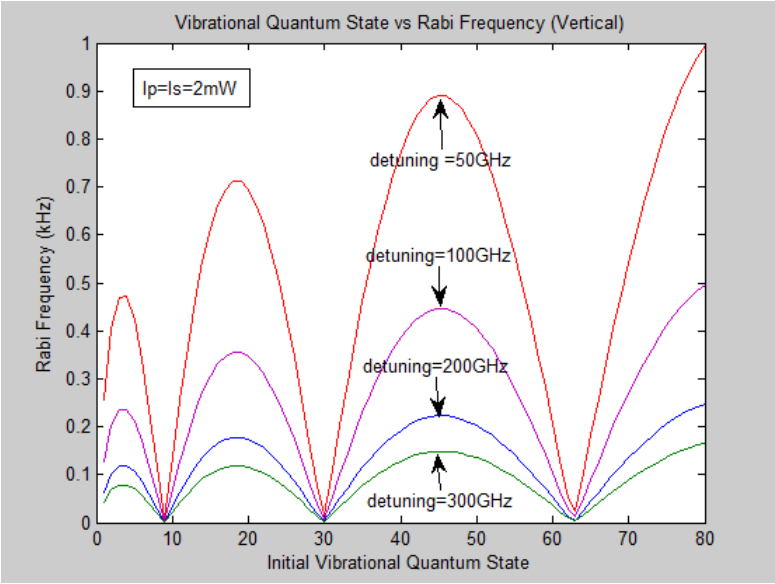

Figure 4.9: Dependence of Rabi frequency on oscillatory state for different detuning in vertical direction. The predicted Rabi frequency varies with oscillatory state as was the case for horizontal direction.

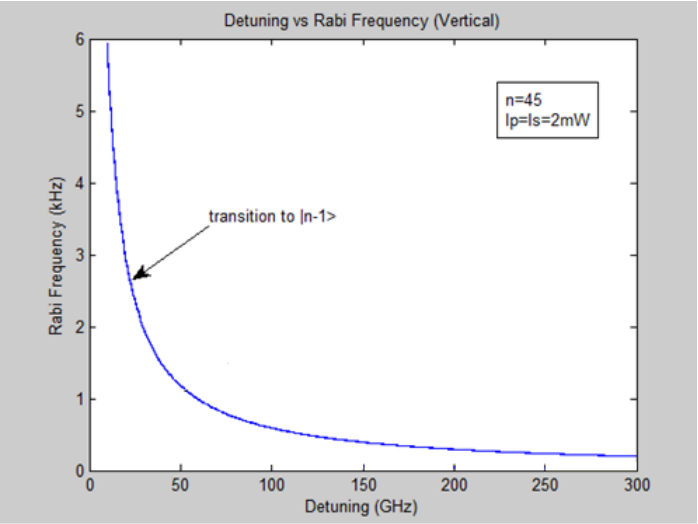

Figure 4.10: Dependence of Rabi frequency, $\Omega_{n\to n-1}$, on the detuning in vertical direction. The third condition of Raman-cooling requires that $\Omega_{n\to n-1} \ll \omega_{rad} \approx 2\pi \cdot 20$ kHz. For this the detuning should be greater than at least 50 GHz.

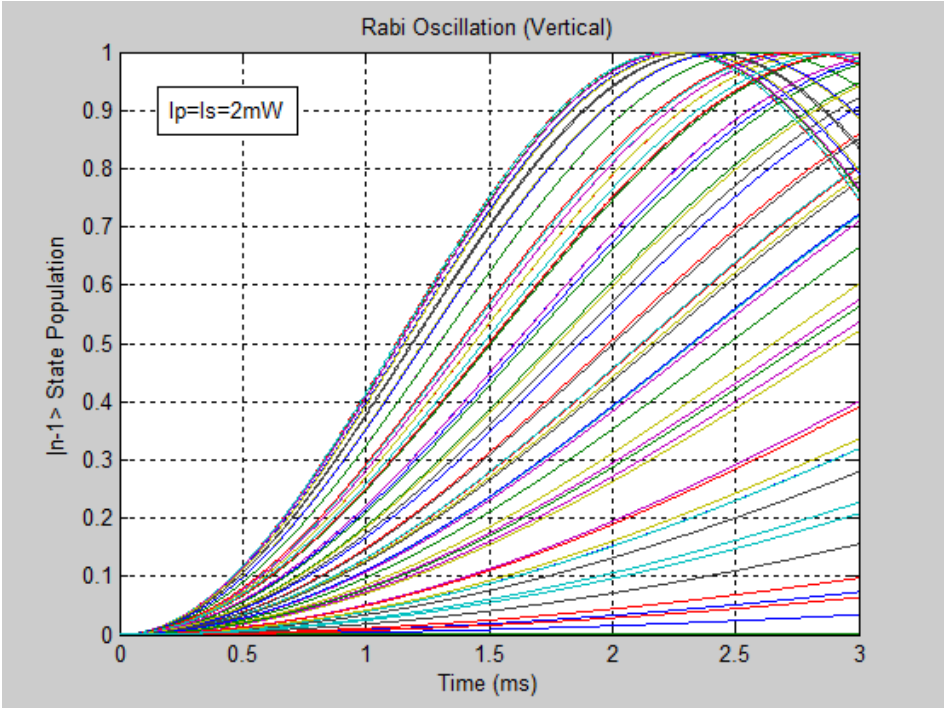

Figure 4.11: Rabi-oscillation for different initial oscillatory states in vertical direction. As Rabi-frequency varies with the oscillatory states, the timing of the optical pumping lasers has to be determined with the highest Rabi-frequency. In this case, the timing should be around 2 ms.

4.7: Conclusion

We have shown that Raman-transition in which an atom with three-level Λ-system undergoes transition from one ground state to the other via a virtual state can cool a trapped atom to its oscillatory ground state. Though it is a three-level system, the system can be reduced to effective two-level system. Rabi-frequency of the effective two-level system has contributions due to the internal and oscillatory states and due to the polarization of laser beams. Cooling is achieved by tuning the laser frequencies so that two-photon resonance to a sideband corresponding to decrease of oscillatory number by 1 and by applying optical pump lasers which preserves the oscillatory states.

In our experiment, the Raman-lasers are not parallel to the quantization axis defined by a magnetic field, and therefore, σ^+-polarization of the lasers are seen as the mixture of $\sigma^{\pm}$- and π-polarizations. Also the atom is expected to exhibit a wide range of Rabi-frequencies depending on the oscillatory states. The timing of the optical pumping lasers is, therefore, not ideal for all the oscillatory states but chosen according to the highest Rabi-frequency. The final oscillatory state will be measured from the intensity of scattered light. The frequency difference of Raman-lasers is fixed exactly by phase-lock loop.

With this, we expect to demonstrate Raman-cooling of cesium atom to the ground oscillatory state.

References

1. P. W. Shor, Polynomial-Time Algorithms for Prime Factorization and Discrete Logarithms on a Quantum Computer, SIAM J.Sci.Statist.Comput. 26 (1997) 1484.
2. H. J. Briegel, T. Calarco, D. Jaksch, J. I. Cirac and P. Zoller, Quantum computing with neutral atoms, J. Mod. Opt., vol. 47, No. 2/3, p. 415-451 (2000).
3. J.I. Cirac and P. Zoller, Quantum Computation with Cold Trapped Ions, Phys. Rev. Lett. 74, 4091-4094 (1995).
4. T. Pellizzari, S. A. Gardiner, J. I. Cirac,and P. Zoller, Decoherence, Continuous Observation, and Quantum Computing: A Cavity QED Model, Phys. Rev. Lett. 75, 3788-3791 (1995).
5. I. L. Chuang, Quantum Computation with Nuclear Magnetic Resonance, in Introduction to Quantum Computation and Information, H. K. Lo et al, editors, 311-339, World Scientifi, Singapore (1998).
6. D. Loss and D. P. DiVincenzo, Quantum Computation with Quantum Dots, Phys. Rev. A, 57, 120 (1998)
7. D. J. Wineland and H. Dehmelt, Bull. Am. Phys. Soc. 20, 637 (1975).
8. A. M. I. Suhaimee, Generation of a donut beam for a tight radial confinement of atoms in a one-dimensional optical lattice, Masterarbeit, Universität Bonn (2010)
9. P. Cprrec, O. Girard, and I. F. Faria, Jr., On the Thermal Contribution to the FM Response of DFB Lasers: Theory and Experiment, IEEE, J. Quantum Electronics, Vol. 30, 2485 (1994)
10. T. Udem, A. Huber, B. Gross, J. Reichert, M. Prevedelli, M. Weitz, and T. W. Hänsch, Phase-Coherent Measurement of the Hydrogen 1S-2S Transiton Frequency with and Optical Frequency Interval Divider Chain. Phys. Rev. Lett, 79, 2646 (1997)
11. G. Santarelli, A. Clairon, S. N. Lea, and G. M.Tino, Phase-locking of two self-seeded tapered amplifier lasers, Opt. Commun. 104, 339 (1994)
12. F. M. Gardner, Phaselock Techniques, second edition, Wiley-Interscience,
13. M. MUELLER, Ramankühlung einzelner Atome, diplomarbeit, Universität Bonn (2001)
14. M. LINDBERG, J. JAVANAINEN, Temperature of a laser-cooled trapped three-level ion, J. Opt. Soc. Am. B, Vol. 3, No. 7, p. 1008-1017, (1986)
15. D. J. WINELAND, W. M. ITANO, Laser cooling of atoms, Phys. Rev. A, Vol. 20, No. 4, p. 1521-1540, (1979)

Acknowledgement

First of all, I would like to thank Prof. Meschede for accepting me into his group and giving me an opportunity to learn further in quantum optics and experimental physics. I would also like to thank Dr. Eversheim for kindly accepting to be the coreferent.

I would like to thank the members and former members of the single group, Artur Widera, Woflgang Alt, Jai-Min Choi, Michal, Leonid, Andreas, Noomen, Andrea and Arif. Your support in experiment, theory and also insight into business of physics were valuable for me.

I also would like to thank Martin Eckstein for sharing his knowledge of OPLL and support in experiment and Amir Moqanaki for his encouragement and presence.

I also would like to thank all members of the group and administrative staff for their kind assistance.

And at last, I would like to thank Universität Bonn for giving me an opportunity to participate in the Master of Science program. I enjoyed variety of learning opportunities it provides, and the last two and a half years have been an invaluable experience. Thank you.

I hereby certify that the work presented here was accomplished by myself and without the use of illegitimate means or support, and that no sources and tools were used other than those cited.

Bonn, ...: